# Typology of the flow structures in dividing open channel flows

Adrien Momplot, Gislain Lipeme Kouyi, Emmanuel Mignot, Nicolas Rivière, Jean-Luc Bertrand-Krajewski

# Typology of the flow structure in dividing open channel flows

ADRIEN MOMPLOT[1], GISLAIN LIPEME KOUYI[1], EMMANUEL MIGNOT[2], NICOLAS RIVIERE[2], JEAN-LUC BERTRAND-KRAJEWSKI[1]

[1] Université de Lyon, INSA de Lyon, LGCIE – Laboratory of Civil & Environnemental Engineering, F-69621 Villeurbanne cedex, FR *Emails: adrien.momplot@insa-lyon.fr (Corresponding Author); gislain.lipeme-kouyi@insa-lyon.fr; jean-luc.bertrand-krajewski@insa-lyon.fr*

[2] LMFA, CNRS-Université de Lyon, INSA de Lyon, Bât. Joseph Jacquard, 20 Avenue Albert Einstein, F-69621 Villeurbanne cedex, FR *Emails: emmanuel.mignot@insa-lyon.fr; nicolas.riviere@insa-lyon.fr*

**ABSTRACT**

The present study reports the occurrence of a new recirculation structure taking place in the lateral branch of a 90° bifurcation flow. This recirculation structure is "helix-shaped" and strongly differs from the typical "closed" recirculation often reported in the literature. The aim of the study is to detail their characteristics using experimental and numerical approaches and to establish a typology, *i.e.* the flow conditions leading to each recirculation structure based on the upstream Froude number and the upstream aspect ratio.

*Keywords:* bifurcation, hydraulic parameters, open-channel flow, RANS model, recirculation structures

## 1 Introduction

Bifurcations of open-channel flows are specific structures frequently encountered in sewer systems or river delta. Bifurcation flows have been widely studied (Grace and Priest, 1958; Shettar and Murthy, 1996; Hsu *et al.*, 2002; Ramamurthy *et al.*, 2007; Mignot *et al.*, 2013; Momplot *et al.*, 2013). Hence, governing parameters of a bifurcation flows are well identified: inlet discharge and discharge repartition in downstream channels. In the literature, the principal challenge for bifurcations lies in the prediction of the flow distribution from the incoming flow towards each outgoing flow. A review of analytical models developed to access such prediction can be found in Rivière *et al.* (2007, 2011). The model proposed by the authors is based on the momentum conservation law as proposed by Ramamurthy *et al.* (1990), suitable stage-discharge relationships for the downstream controls in the outflow channels and an empirical correlation obtained through experimental data.

Nevertheless, understanding the behavior of the flow structures within the bifurcation is also important, as they strongly impact pollutant or sediment transport and mixing

processes. The general pattern of a steady subcritical 3-branch bifurcation is described by Neary *et al.* (1999). A three-dimensional recirculating region develops in the lateral branch and secondary flows appear in both outlets. Mignot *et al.* (2014) detailed the mixing layer taking place at the frontier between the main flow and the recirculation zone in the lateral branch. Recirculation zones, also defined as bubbles, are encountered in various geometries as listed by Li and Djilali (1995).

Regarding specifically the recirculation zone, authors such as Kasthuri and Pundarikanthan (1987), Shettar and Murthy (1996) and Neary *et al.* (1999) sketch the recirculation zone (in top view) as a closed semi-elliptic region developing along the upstream wall of the lateral branch with maximum length and width at the free-surface and minimum extensions in the near-bed region. Kasthuri and Pundarikanthan (1987) and Shettar and Murthy (1996) respectively measure and compute the free-surface length and width of this recirculation zone. The authors agree that as the relative lateral discharge increases, the dimensions of the recirculation zone decreases. Neary *et al.* (1999) then compute flow configurations with varying channel width ratios and dimensionless water depths and exhibit varying characteristics of the recirculation zone pattern without clear explanation of the different types of recirculation zones.

The aim of the present paper is twofold: first to describe the two main flow structures that can be observed in the lateral branch of a 90° bifurcation and second to determine the flow conditions for which each structure is observed. The paper is organized as follows: after presenting the experimental and numerical approaches, the characteristics of the different types of recirculation zones are described based on two measured and computed flows (F1 and F2) and finally a campaign of numerical simulations (including 16 different cases) is led in order to establish the flow typology.

## 2 Material and methods

### *2.1 Experimental set up*

The experimental set-up (see Fig. 1) is a horizontal 3-branch equal width ($B$=30 cm) glass open-channel bifurcation of 2 and 2.6 meters long channels for the inlet and both outlet respectively. Boundary conditions are the inlet discharge $Q_U$ (measured by a flow-meter in the pumping loop) and the weir crest height $C_D$ and $C_L$ at the downstream end of each of the two outlet channels. The water depths in the upstream, lateral and downstream branches are defined as $h_U$, $h_L$ and $h_D$ respectively and are measured using a digital point gauge. The discharge distribution $Q_L/Q_U$ in the bifurcation is measured through an additional flow-meter in the pumping loop. In the studied cases, flow conditions are sub-critical everywhere. Details about this set-up are available in Mignot *et al.* (2013 and 2014).

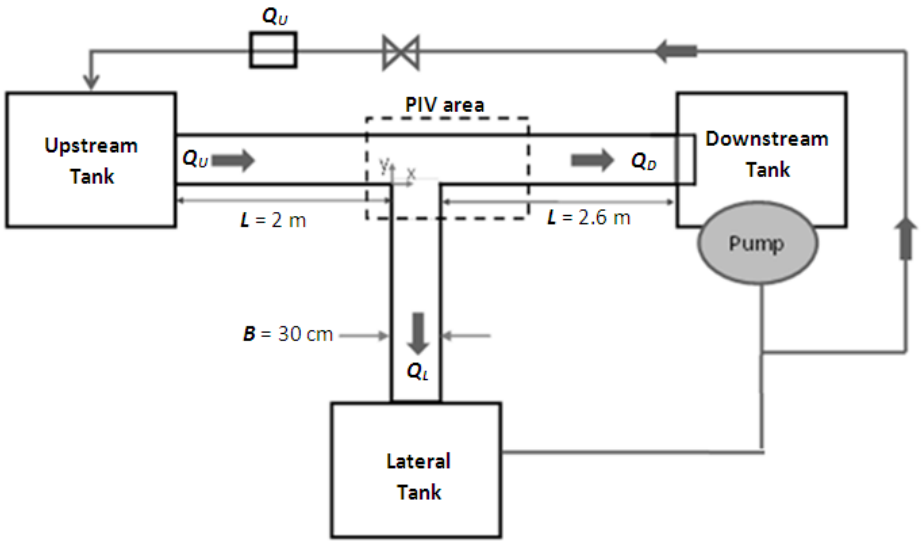


Figure 1. Experimental set up used for flow validation.

## 2.2 *Modelling strategy*

Numerical simulations are performed under the commercial software ANSYS Fluent version 14.0, following the modelling strategy proposed by Momplot *et al.* (2013) for computing bifurcation flow F0 (see Table 1), these simulations are confronted with PIV measurements of the horizontal velocity fields (see Fig. 2). Overall performances are fair. Additionally, simulated discharge repartition and measured discharge repartition shows fair agreement (differences are less than 10%).

Table 1. Characteristics of the validated flow.

| Flow id. | Inlet discharge $Q_U$ ($L.s^{-1}$) | Weir crest height $h_{crest}$ (m) | Discharge distribution ($Q_L/Q_U$) | Froude Number in upstream channel (-) | Upstream aspect ratio $B/h_U$ (-) |
|---|---|---|---|---|---|
| F0 | 4 | 0.12 | 0.51 | 0.102 | 2.5 |

The model solves the RANS (Reynolds Averaged Navier-Stokes) equations using the Volume of Fluid - VOF -method for computing the free-surface curve and a Reynolds stress model - *RSM* - as turbulence model for system closure (see Launder *et al.*, 1975). *Scalable* wall-functions (see Grotjans and Menter, 1998) are used for walls; a uniform velocity $U_{Inlet}$ is set at the inlet cross-section; atmospheric pressure $P_0$ is set at the top of the computational domain and at outlets. Crest heights are explicitly represented in the mesh. After the weirs, standard pressure outlet conditions are set. Discretisation scheme use for pressure is *Body-Force Weighted* and *Second-Order Upwind* for other variables. Pressure-velocity coupling algorithm is *PISO*.

Mesh independency is verified using the grid convergence index (GCI) defined by Roache (1994) as:

$$GCI_X = \frac{(X_F - X_C) \cdot r^p}{r^p - 1}$$

Equation 1

With : -$GCI_X$: the simulation error on variable $X$ due to the fine mesh (dimension of $X$), $X$ can be a discharge, a water depth, a velocity, etc.

-$X_F$: the simulated variable $X$ for the fine mesh (dimension of $X$)

-$X_C$: the simulated variable $X$ for the coarse mesh (dimension of $X$)

-$r$: the ratio $\frac{N_F}{N_C}$, $N_F$ being the fine mesh number of cells and $N_C$ the coarse mesh number of cells (dimensionless)

-$p$: the discretisation schemes order (dimensionless).

The $GCI_X$ value is an estimator of the error committed on the true variable X value that is due to the mesh. Mesh independency is obtained when the relative error is below 5%.

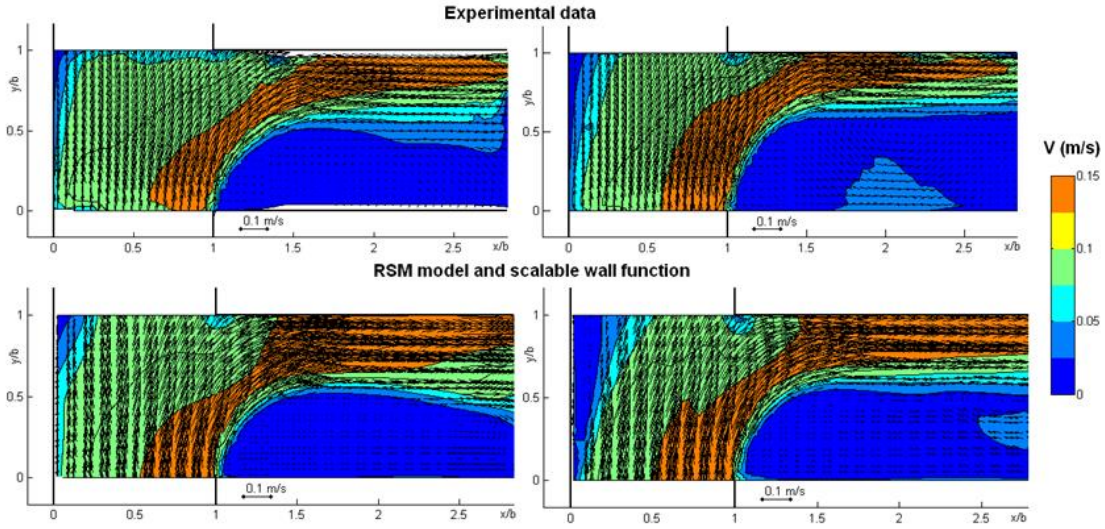


Figure 2. Confrontation between PIV measurements of horizontal velocity fields (top) and simulated horizontal velocity fields (bottom) for two elevation: z = 4 cm (left) and z = 9 cm (right).

## 3 Flow structure description

Table 2. Cases F1 and F2 studied experimentally and numerically exhibiting respectively a "helix-shaped" recirculation and a "closed" recirculation structure in the lateral branch.

| Flow id. | Inlet discharge $Q_U$ (L.s$^{-1}$) | Weir crest height $h_{crest}$ (m) | Discharge distribution ($Q_L/Q_U$) | Froude Number in upstream channel (-) | Upstream aspect ratio $B/h_U$ (-) |
|---|---|---|---|---|---|
| F1 | 8 | 0.09 | 0.47 | 0.218 | 2.50 |
| F2 | 4 | 0.025 | 0.50 | 0.448 | 6.69 |

Table 3. GCI analysis for flow F1 and F2.

| | F1 -$h_{crest}$ = 9 cm $Q_U$ = 8 L/s- | | | |
|---|---|---|---|---|
| | Base mesh | GCI mesh | Absolute mesh error | Relative mesh error |
| Mesh size (cells) | 738000 | 461500 | - | - |
| $Q_D$ ($m^3.s^{-1}$) | 4.320 | 4.352 | 0.053 | 0.012 |
| $Q_L$ ($m^3.s^{-1}$) | 3.743 | 3.706 | 0.061 | 0.016 |
| $U_{moy\text{-}U}$ ($m.s^{-1}$) | 0.237 | 0.24 | 0.005 | 0.021 |
| $U_{moy\text{-}L}$ ($m.s^{-1}$) | 0.1104 | 0.1108 | 0.001 | 0.006 |
| | F2 -$h_{crest}$ = 2.5 cm $Q_U$ = 4 L/s- | | | |
| | Base mesh | GCI mesh | Absolute mesh error | Relative mesh error |
| Mesh size (cells) | 756000 | 412500 | - | - |
| $Q_D$ ($m^3.s^{-1}$) | 2.276 | 2.343 | 0.110 | 0.048 |
| $Q_L$ ($m^3.s^{-1}$) | 1.762 | 1.744 | 0.030 | 0.017 |
| $U_{moy\text{-}U}$ ($m.s^{-1}$) | 0.388 | 0.379 | 0.015 | 0.038 |
| $U_{moy\text{-}L}$ ($m.s^{-1}$) | 0.211 | 0.21 | 0.002 | 0.008 |

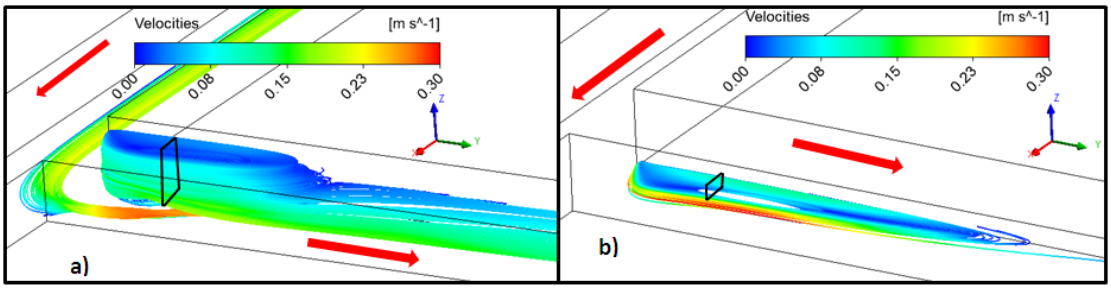


Figure 3. Two flow structures in the lateral branch of a bifurcation flow: a) a helix-shaped recirculation for flow F1 and, b) a closed recirculation for F2. Drawn streamlines are the ones going through the white plane located in the lateral branch at a distance equal to 1B from the entry section, covering the whole water depth and extending transversally from the left bank to the streamlines that separates at the corner between the upstream and lateral branches. This plane permits to enclose the whole recirculation. Red arrows indicate the main flow directions.

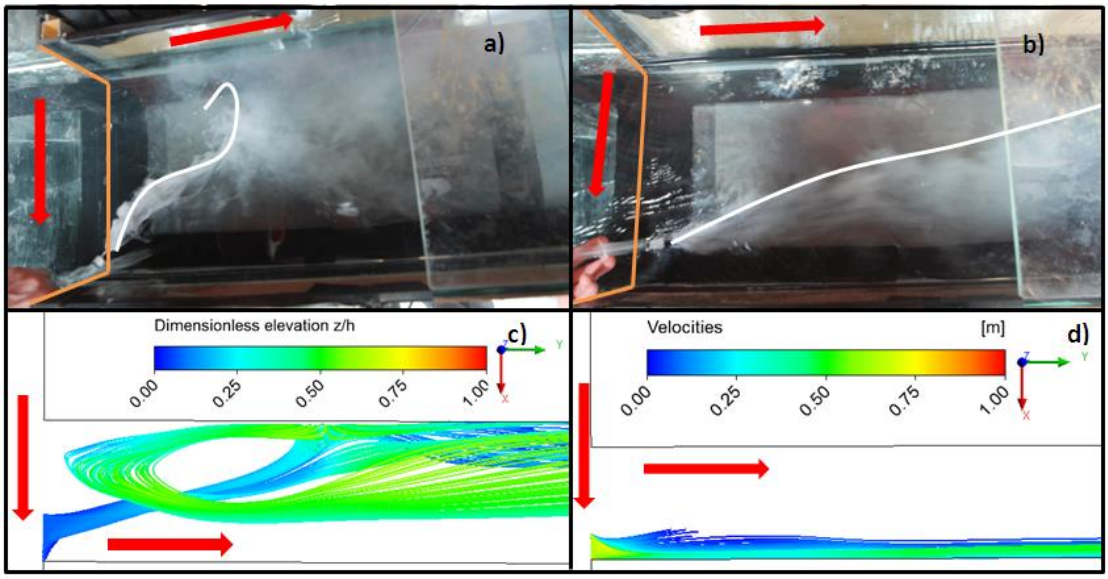


Figure 4. Laboratory and simulation observations of two different flow structures in the lateral branch of two bifurcation flows: F1 (a-c) and F2 (b-d). (a-b) show experiments, (c-d) show numerical streamlines colored by the dimensionless elevation $z/h_L$ (from blue, being the bottom of the channel; to red, being the free-surface). For (a-b), a white dye tracer is injected in the downstream corner of the lateral channel, near the bottom, the white line represents the limit of the tracer extension, red arrows indicate flow directions and orange lines mark the inlet section of the lateral branch.

Among all studied flows, two recirculation structures could be observed. Table 2 presents two flow cases investigated numerically and experimentally, each one exhibits a different recirculation structure: a so-called “helix shaped” for F1 and a “closed” one for F2. Fig. 4 shows numerical results for these flow cases and particularly the behaviour of some selected streamlines. Fig. 4 compares experimental observations for the two flow cases regarding the transport of white dye tracer in the lateral branch and numerical streamlines obtained through RANS simulations. In both cases, injection takes place near the bottom part of the downstream corner region. These results confirm the fair agreement between simulated and measured flow patterns. Additionally, results of the GCI analysis displayed in Table 3 indicates that meshes used to compute both flows are efficient for the prediction of discharge and bulk velocities in the lateral branch. Surprisingly, the mesh for flow F2 is less efficient for discharge and velocities representation in the upstream branch than the mesh for flow F1.

The two figures permit to describe both recirculation structures:

- The closed recirculation observed for flow F2 is a 2D semi-elliptic closed region developing along the upstream wall of the lateral branch as described in the literature: no flow enters or leaves this region and it is of larger streamwise and transverse extension at the free-surface than near the bed (Fig. 3b). Consequently, the streamlines starting from the

downstream corner of the intersection remain quite parallel to the banks of the lateral channel towards downstream and do not interact with the recirculation zone (Fig. 4b).

- The helix-shaped recirculation observed for flow F1 is a 3D ascendant flow (see Fig. 3a and 4c): i. supplied by the bottom flow of the upstream channel, ii. entering the lateral branch near the bottom part of the downstream corner area, iii. approaching the opposite (upstream) wall of the lateral branch, iv. raising towards the free-surface, first in the direction of the intersection (towards upstream) and then towards downstream along center of the branch. v. escaping towards downstream in the upstream half of the branch. Consequently, the streamlines starting from the downstream corner of the intersection enter the recirculation structure (Fig. 4a). These two distinct flow structures corroborate the different streamlines plots near the bottom reported by Neary *et al.* (1999) in their figure 10 and the pathlines in their figure 11c.

## 4 Flow typology

In order to establish the flow conditions for which each recirculation structure is observed, a flow typology is established following the parameters obtained through dimensional analysis. Using the same approach as Mignot *et al.* (2013) and assuming (as for the authors) that the flow is turbulent (see Table 10) and smooth, the 8 parameters governing the flow characteristics are: the three discharges ($Q_U$, $Q_L$, $Q_D$), the three water depths ($h_U$, $h_L$, $h_D$) and the two weir crest heights ($C_D$, $C_L$). Mass conservation equation ($Q_U = Q_L + Q_D$) permits to remove one parameter ($Q_L$); both known stage discharge equations ($h_D = f(Q_D, C_D)$ and $h_L = f(Q_L, C_L)$) permit to remove $h_L$ and $C_D$; the momentum equation introduced by Ramamurthy *et al.* (1990) permits to remove $h_D$; the empirical closure equation introduced by Rivière *et al.* (2007) permits to remove $Q_D$; finally, the following simplification considered in the present work $C_D$=$C_L$ permits to remove $C_L$. We end up with the two remaining parameters $Q_U$ and $h_U$, which can be transformed (see Mignot *et al.*, 2013) as dimensionless independent parameters: upstream Froude number $Fr_U$ and upstream aspect ratio $B/h_U$. Note that the present simplification $C_D = C_L$ is responsible for the reduction of independent parameters from 3 in Mignot *et al.* (2013) to 2 in the present work and leads to a discharge distribution $Q_L/Q_U$ of about 45 to 55%.

The aim of the part being a flow typology assessment for a recirculation zone, a quick look at others recirculation zone typologies is needed. There is many situations leading to a recirculation zone (listed by Li and Djilali, 1995). For each of these situations, a flow typology can be established by studying specific forces configurations. For example, Chu et al. (2004) establish a typology for a recirculation zone where confinement and friction are the determining forces. Dufresne et al. (2010) also establish a recirculation zone typology in rectangular shallow reservoirs, where inertial forces and pressure/water depth gradients are

determining forces. These two cases lead to two different typologies. In the present case, the suspected determining forces are centrifugal force and pressure force: when the centrifugal force effect is significant, we can observe the helix-shaped recirculation because of the pressure force induce by the centrifugal force (see Fig. 5). It is similar to the tea-leaves effect.

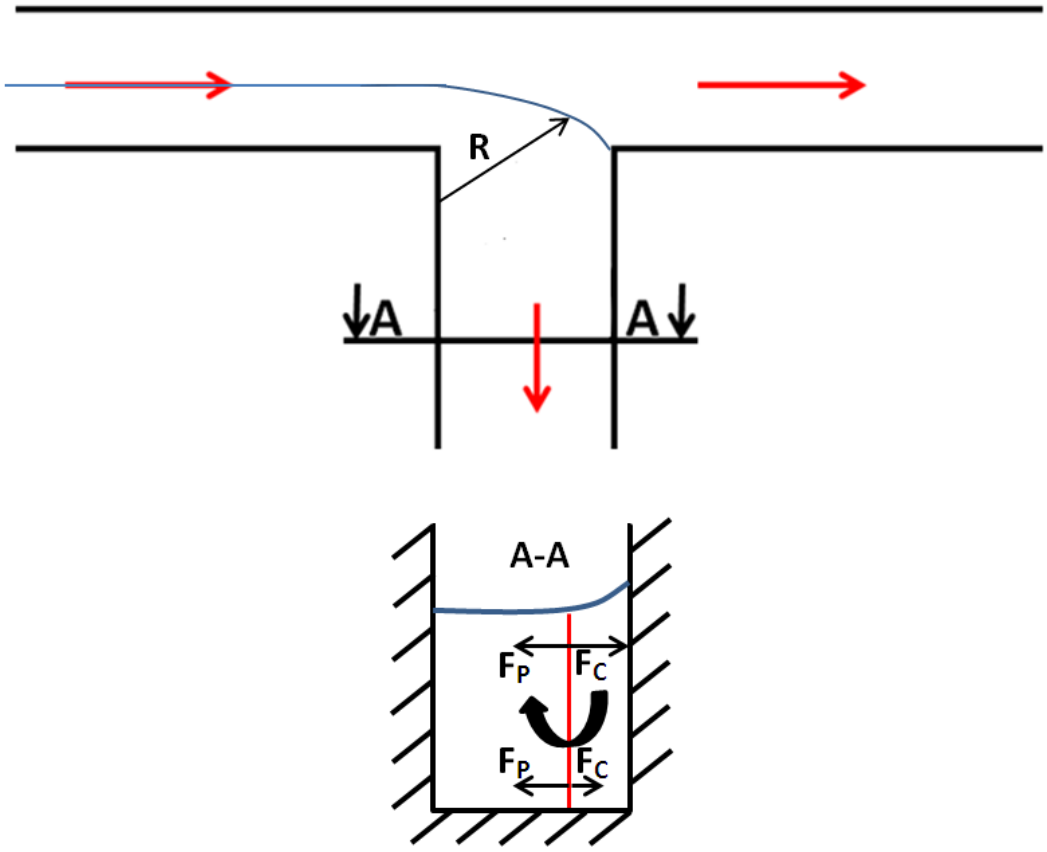


Figure 5. Forces balance in a lateral branch cross-section. Red arrows indicate flow directions. $F_C$ is the volume centrifugal force (N.m$^{-3}$), $F_P$ the volume pressure force (N.m$^{-3}$). Blue line indicates the free surface in the cross-section and $R$ is the curvature radius of the separation.

Two forces are defined in the lateral branch cross-section A-A (see Fig. 5) as follow:

$$F_C = \rho \frac{U_U^2}{R}$$ Equation 2

$$F_P = \rho g$$ Equation 3

Where:
- $F_C$: the centrifugal force (N.m$^{-3}$)
- $U_U$: the mean velocity in the upstream channel (m.s$^{-1}$)
- $R$: the curvature radius of the separation (m)
- $F_P$: the pressure force (N.m$^{3}$)
- $g$: the acceleration of gravity (= 9.81 m.s$^{-2}$)

A comparison between the two defined forces gives:

$$\frac{F_C}{F_P} = \frac{\rho \frac{U_U^2}{R}}{\rho g} = \frac{U_U^2}{Rg}$$

Equation 4

It is possible to assimilate $R$ to the channel width $B$. Equation 4 becomes:

$$\frac{F_C}{F_P} = \frac{U_U^2}{Bg} = \frac{U_U^2}{\frac{B}{h_U} \cdot g h_U} = \frac{Fr_U^2}{\frac{B}{h_U}}$$

Equation 5

With: -$h_U$: the water depth in the upstream channel (m)

Equation 5 indicates that a relationship between the squared Froude number in the upstream channel $FrU^2$ and the upstream aspect ratio B/hU can determine the flow topology. A numerical campaign is led to investigate this possible relationship.

Table 4 presents the numerical campaign, comprising 16 flow cases, led to establish the flow typology. For each case, Froude number is upstream channel $Fr_U$ is defined as:

$$Fr_U = \frac{U_U}{\sqrt{g \cdot h_U}} \in [0.035; 0.558]$$

Reynolds number in upstream channel ReU is defined as:

$$Re_U = \frac{4 \cdot U_u \cdot B \cdot h_U}{\upsilon \cdot (B + 2 \cdot h_U)} \in [7400; 103900]$$

With : -$U_U$: the mean velocity in the upstream channel ($m.s^{-1}$)
-$B$: the channel width (m)
-$h_U$: the upstream channel water depth (m)

All tested cases are thus subcritical and turbulent (see Table 4).

For this campaign, the crest height in both outlet branches $C_D$ *and* $C_L$ *(*$C_D$ = $C_L$*)* and the upstream discharge $Q_U$ are the two varying boundary conditions which permit to vary the two independent parameters: $Fr_U$ and $B/h_U$.

Table 4. Simulated cases for the typology numerical campaign.

| | Crest height in downstream branches $h_{crest}$ (m) | Inlet discharge $Q_U$ ($L.s^{-1}$) | Flow distribution ($Q_L/Q_U$) | Reynolds Number in upstream branch $Re_U$ (-) | Froude Number in upstream branch $Fr_U$ (-) | Upstream aspect ratio $B/h_U$ (-) |
|---|---|---|---|---|---|---|
| Case 1 | 0.03 | 1 | 0.485 | 11066 | 0.204 | 10.00 |
| Case 2 | 0.03 | 4 | 0.45 | 40240 | 0.400 | 6.20 |
| Case 3 | 0.03 | 8 | 0.454 | 75340 | 0.540 | 4.76 |
| Case 4 | 0.03 | 12 | 0.345 | 88130 | 0.558 | 4.29 |
| Case 5 | 0.05 | 1 | 0.505 | 9700 | 0.095 | 6.12 |
| Case 6 | 0.05 | 4 | 0.481 | 39810 | 0.260 | 4.41 |

| | | | | | | |
|---|---|---|---|---|---|---|
| Case 7 | 0.05 | 8 | 0.457 | 79070 | 0.333 | 3.84 |
| Case 8 | 0.05 | 12 | 0.433 | 103903 | 0.486 | 3.30 |
| Case 9 | 0.07 | 1 | 0.511 | 8504 | 0.052 | 4.16 |
| Case 10 | 0.07 | 4 | 0.472 | 35950 | 0.172 | 3.37 |
| Case 11 | 0.07 | 8 | 0.459 | 67260 | 0.289 | 3.06 |
| Case 12 | 0.07 | 12 | 0.555 | 80810 | 0.352 | 2.75 |
| Case 13 | 0.09 | 1 | 0.521 | 7400 | 0.035 | 3.33 |
| Case 14 | 0.09 | 4 | 0.488 | 34310 | 0.130 | 2.73 |
| Case 15 | 0.09 | 8 | 0.468 | 63070 | 0.218 | 2.50 |
| Case 16 | 0.09 | 12 | 0.474 | 96800 | 0.266 | 2.00 |

Fig. 6 shows the distribution of each recirculation structure, according to two parameters: squared upstream Froude number $Fr_U^2$ and upstream aspect ratio $B/h_U$. Both regions are clearly separated from each other: a linear – at least with the present set of experiments – oblique boundary separates the two types. For low $Fr_U^2$ and high $B/h_U$ values, the closed recirculation takes place whilst for high $Fr_U^2$ and low $B/h_U$ values, the helix-shaped recirculation occurs.

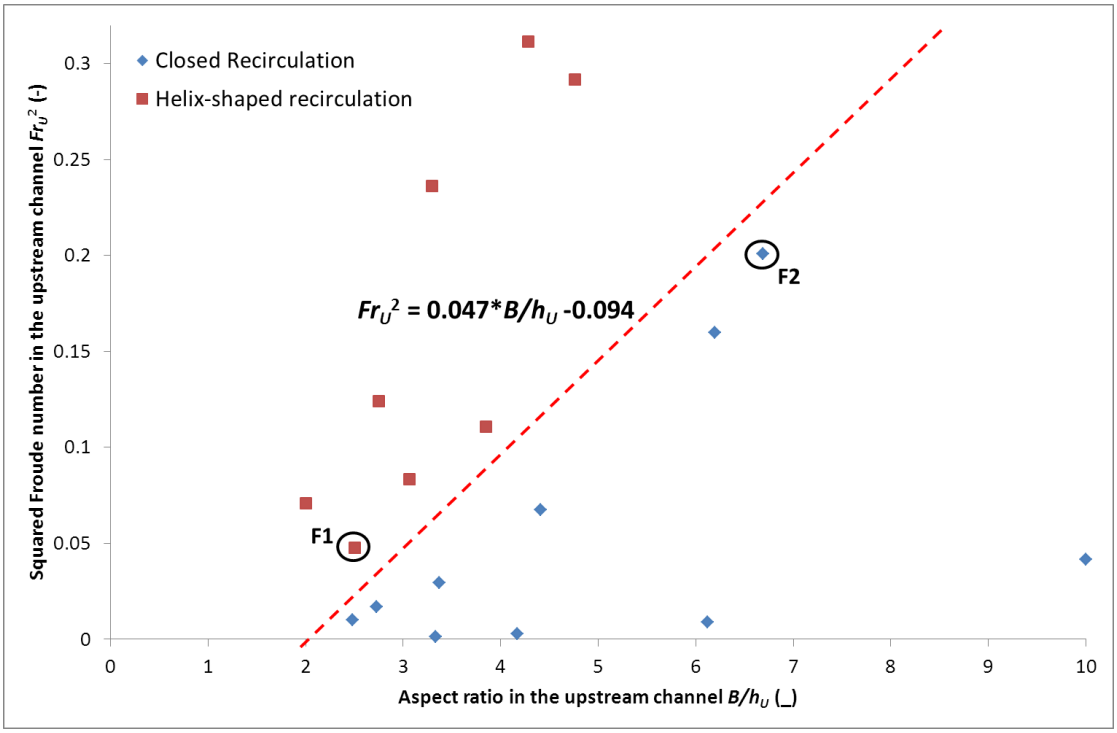


Figure 6. Flow typology in the lateral branch. Flow F1 and F2 are circled. The red-dashed line represents the boundary between a classic recirculation in lateral branch and a helix-shaped one.

## 5 Conclusions and perspectives

The present papers aimed at defining the flow patterns occurring in the lateral branch of an open-channel bifurcation. A typology comprising two flow structures was established based

on the characteristics of the recirculation zone. The two structures are named i. “closed recirculation”, similar to the flow pattern previously described in the literature and ii. “helix-shaped recirculation” for which the flow pattern strongly differs and is described in the present paper. Both structures were observed using both experimental and numerical approaches. Following the assumptions of a smooth and turbulent flow regime and equal weir crest heights at both outlets, the typology is based on the comparison between centrifugal force effect and pressure force effect by the mean of squared upstream Froude number $Fr_U^2$ and upstream aspect ratio $B/h_U$ and exhibits two clear regions of recirculation structure occurrence.

As perspectives, bed friction effect should be investigated, as well as Reynolds number effect. As the define flow topology depends on curvature radius of the separation, the effect of channel width ratio and discharge repartition will have an effect and should also be investigated.

**Acknowledgements**

These works are part of the laboratory of excellence IMU (Smartness on Urban Worlds) and the OTHU (Field Observatory for Urban Hydrology) at Lyon. Authors would like to thank: the French ministry of research for the Ph.D. funding and the ANR (National Agency for research) project funding (ANR-11-ECOTECH-007-MENTOR) and the INSU (National Institute for Universe Science, project EC2CO-Cytrix 2011 project No 231).

**Notations**

$B$ = channel width (m)
$C_L$ = crest height in the lateral branch (m)
$C_D$ = crest height in the downstream branch (m)
$F_C$ = centrifugal force ($N.m^{-3}$)
$F_P$ = pressure force ($N.m^{-3}$)
$Fr_U$ = Froude number in upstream channel (-)
$GCI_X$ = grid convergence index value for variable $X$ (dimension of variable $X$)
$h_U$ = water depth in the upstream channel (m)
$h_L$ = water depth in the lateral branch (m)
$h_D$ = water depth in the downstream branch (m)
$h_{crest}$ = crest height for case F1 and F2 (m)
$k$ = wall roughness (m)
$N_C$ = number of cells of the coarse mesh (-)
$N_F$ = number of cells of the fine mesh (-)
$P_0$ = atmospheric pressure (Pa)
$Q_U$ = upstream discharge ($L.s^{-1}$)
$Q_L$ = lateral branch discharge ($L.s^{-1}$)
$Q_D$ = downstream branch discharge ($L.s^{-1}$)
$r$ = cell number ratio between fine mesh and coarse mesh (-)
$R$ = curvature radius of the separation zone (m)
$Re_U$ = Reynolds number in upstream branch (-)

286 $U_{Inlet}$ = numerical velocity set at the inlet cross-section of the upstream channel ($m.s^{-1}$)
287 $U_U$ = mean velocity in the upstream channel ($m.s^{-1}$)
288 $X_C$ = value of variable X for coarse mesh (variable)
289 $X_F$ = value of variable X for fine mesh (variable)
290 $z$ = elevation (m)
291 $\nu$ = viscosity of water (= $1.10^{-6}$ $m^2.s^{-1}$)

# 292 References


293 Chu, V. H., Liu, F., & Altai, W. (2004). Friction and confinement effects on a shallow
294 recirculating flow. *Journal of Environmental Engineering and Science*, 3(5), 463-475.
295 Dufresne, M., Dewals, B. J., Erpicum, S., Archambeau, P., & Pirotton, M. (2010).
296 Experimental investigation of flow pattern and sediment deposition in rectangular
297 shallow reservoirs. *International Journal of Sediment Research*, 25(3), 258-270.
298 Grace, J. L. & Priest, M. S. (1958). Division of flow in open channel junctions. *Bulletin*
299 *No.31*. *Engineering Experiment Station*, Alabama Polytechnic Institute.
300 Grotjans H. & Menter F. R. 1998. Wall functions for industrial applications. In Proceedings
301 of *Computational FluidDynamics'98*, *ECCOMAS*, 1(2), Papailiou KD (ed.). Wiley:
302 Chichester, U.K.. 1112–1117
303 Hsu, C. C., Tang, C. J., Lee, W. J. & Shieh, M. Y. (2002). Subcritical 90 equal-width open-
304 channel dividing flow. *Journal of Hydraulic Engineering*, 128(7), 716-720.
305 Kasthuri B. & Pundarikanthan N. V. (1987). Discussion of "Separation zone at open channel
306 junctions". *Journal of Hydraulic Engineering*, 113(4), 543.
307 Launder B. E., Reece G. J. & Rodi W. (1975). Progress in the Development of a Reynolds-
308 Stress Turbulence Closure. *Journal of Fluid Mechanics*. 68(3). 537–566
309 Li X. & Djilali N. (1995). On the scaling of separation bubbles. *JSME international journal.*
310 *Series B, fluids and thermal engineering*, 38(4), 541-548.Mignot, E., Zeng, C.,
311 Dominguez, G., Li, C. W., Rivière, N. & Bazin, P. H. (2013). Impact of topographic
312 obstacles on the discharge distribution in open-channel bifurcations. Journal of
313 Hydrology, 494, 10-19.
314 Mignot, E., Doppler, D., Riviere, N., Vinkovic, I., Gence, J. N. & Simoens, S. (2014).
315 Analysis of flow separation using a local frame-axis: application to the open-channel
316 bifurcation. *Journal of Hydraulic Engineering*. 280-290.
317 Momplot, A., Lipeme Kouyi, G., Mignot, E., Rivière, N. & Bertrand-Krajewski, J.-L. (2013)
318 URANS Approach for Open Channel Bifurcation Flows Modelling. *7th International*
319 *Conference on Sewer Processes and Network*, Sheffield, August 2013, 8 pages.
320 Neary, V. S., Sotiropoulos, F. & Odgaard A. J. (1999). Three-dimensional numerical model
321 of lateral intake inflows. *Journal of Hydraulic Engineering*, 125(2), 126-140.

322 Ramamurthy, A. S., Tran, D. M. & Carballada, L. B. (1990). Dividing flow in open channels.
323 *Journal of Hydraulic Engineering*, 116(3), 449-455.
324 Ramamurthy, A. S., Qu, J. & Vo, D. (2007). Numerical and experimental study of dividing
325 open-channel flows. *Journal of Hydraulic Engineering*, 133(10), 1135-1144.
326 Rivière, N., Travin, G. & Perkins R. J. (2007). Transcritical flows in open channels junctions.
327 *Proceedings, 32nd IAHR Congress*, Venice, Italy, IAHR, paper SS05-11.
328 Rivière, N., G. Travin, and R. J. Perkins (2011), Subcritical open channel flows in four branch
329 intersections, *Water Resour. Res.*, 47, W10517, doi:10.1029/2011WR010504.
330 Shettar, A. S. & Keshava Murthy, K. (1996). A numerical study of division of flow in open
331 channels. *Journal of Hydraulic Research*, 34(5), 651-675.